A Simplified Transient Model of Surge Protective Devices Employing Varistors

A. Y. Hadjicostas, E. T. Staikos, G. D. Peppas, T. E. Tsovilis

***Abstract*—This work provides a simplified transient model for low-voltage DIN rail surge protective devices (SPDs), accounting for their resistive, inductive, and capacitive behavior. The time-domain modeling approach is based on impulse current and sinusoidal voltage experiments. The lumped-circuit model is implemented in the ATP-EMTP environment and yields results in satisfactory agreement with the experimentally derived residual voltage and energy absorption of commercially available DIN rail SPDs for single- and three-phase installations. The proposed model can be used for evaluating the protection level and maximum residual voltage of SPDs under standard and non-standard surge currents and can be an effective tool employed in insulation coordination studies of power systems.**

***Keywords*: ATP-EMTP, impulse currents, metal-oxide varistor, residual voltage, surge protection.**

I. Introduction

LIGTHNING is one of the main causes of power grid disturbances and faults, resulting in power quality issues, power delivery failures, and building permanent damages [1]. The economic and social adverse consequences of lightning are more significant today than in the past due to the introduction of vulnerable, dispersed renewable energy sources and power & data networks integrated into smart grids [2]. Lightning-related failures have a great financial impact; economic losses are in the order of 200 M€ per year in Germany, according to the German Insurance Association [3]. Thus, the effective surge protection of critical infrastructure and equipment is a hot topic and a challenge of crucial importance so as to cope with the high standards of the necessary reliability and resiliency of modern power grids [4], [5].

For the surge protection of low-voltage power systems, typically, DIN rail surge protective devices (SPDs) employing varistors are installed to distribution panels; SPDs divert the lightning current to the ground and limit the overvoltages to values lower than the withstand voltage of protected equipment. Modeling the non-linear transient behavior of SPDs is a formidable task [6]-[8] since (i) integration of non-linear elements in time-domain simulations is, in general, a challenging process [9], [10] and (ii) the physics of current conduction via metal-oxide varistors is still an open topic [11], [12]. Nevertheless, low-voltage varistor-based surge protective devices are commonly modeled in electromagnetic transient simulation programs following: (i) a simplified purely resistive approach based on the voltage-current characteristic of integrated varistors [13], [14] and/or (ii) a frequency-dependent approach employing lumped-circuit elements, that are mainly developed for gapless high-voltage surge arresters [15]-[17].

The implementation of these models, based on public data provided by low-voltage SPDs manufacturers in datasheets, is practically impossible and the accuracy of these modeling approaches in reproducing the transient performance of low-voltage SPDs is dubious [18]-[20].

This work introduces a simplified electromagnetic transient model for varistor-based SPDs, accounting for their resistive, inductive, and capacitive behavior. The proposed time-domain modeling approach is based on impulse current and sinusoidal voltage experiments on commercially available DIN rail SPDs, commonly installed in Europe; the lumped-circuit model is developed based on a wide range of surge currents up to 40 kA and sinusoidal voltages up to 1 kHz. The proposed model is implemented in the ATP-EMTP environment and yields results in satisfactory agreement with the experimentally derived residual voltage and energy absorption, which are both crucial for the quality of surge protection and SPDs lifetime estimation [21], [22]. It is shown that the proposed model can be used for evaluating the protection level and maximum residual voltage of SPDs under standard and non-standard surge currents, and it can be an effective tool for insulation coordination studies employing transient simulations [23], [24].

II. Devices Under Test and Experimental Arrangements

A. Surge Protective Devices Under Test

Fig. 1 depicts the DIN rail low-voltage surge protective devices (SPDs) under test and their corresponding single-line diagrams. The SPDs under study are Class II according to IEC 61643-11[25], and their basic electrical characteristics are presented in Table I. The protection mode under investigation is the line to neutral mode (L_x-N), where a metal-oxide varistor (MOV) is employed with a maximum discharge current capability of 40 kA, 8/20 μs (Fig. 1, Table I).

The DIN rail SPDs under study are commercially available and commonly employed in distribution panels of TT and TN-S low-voltage systems in Europe per IEC 61643-12 [26]. Pluggable modules are used in single-pole and four-pole

A. Y. Hadjicostas, E. T. Staikos and T. E. Tsovilis are with the High Voltage Laboratory, School of Electrical & Computer Engineering, Aristotle University of Thessaloniki, Thessaloniki, 541 24 Greece (e-mail: chatzikag@ece.auth.gr, evstaikos@ece.auth.gr, tsovilis@auth.gr). George D. Peppas is with Raycap S.A., Industrial Area of Drama 66100, Drama, Greece (e-mail: peppas@upatras.gr).

Paper submitted to the International Conference on Power Systems Transients (IPST2023) in Thessaloniki, Greece, June 12-15, 2023.

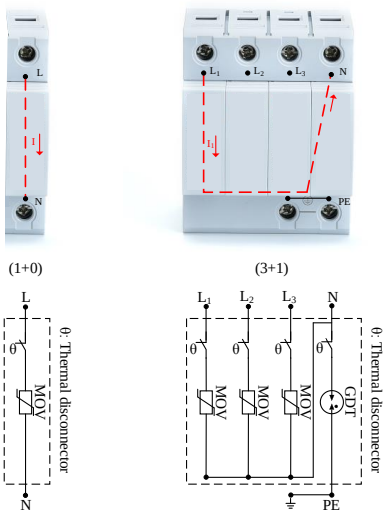

Fig. 1. Low-voltage DIN rail SPDs employing metal-oxide varistors between line and neutral and gas discharge tube between neutral and ground.

TABLE I
SURGE PROTECTIVE DEVICES ELECTRICAL CHARACTERISTICS
(LINE TO NEUTRAL)

Maximum Continuous Operating Voltage (rms), U_C (V)	275
Voltage Protection Level, U_p (V)	1500
Nominal Discharge Current, I_n (kA), 8/20 μs	20
Maximum Discharge Current, I_{max} (kA), 8/20 μs	40

configurations for single-phase and three-phase power systems; the pluggable modules under test were selected to exhibit the same non-linear impedance in order to evaluate the effect of the SPD configuration (bases 1+0 and 3+1 in Fig. 1) on the protective characteristics per protection mode (L-N, L1-N, L2-N, L3-N). These SPD configurations (1+0 and 3+1) were employed in investigations since they involve the minimum (L-N) and maximum (L1-N) length of surge current paths between line and neutral, as denoted by dashed red arrows in Fig. 1, when compared with 2+0, 3+0, and 1+1 SPDs per IEC 60364-5-53 [27].

B. Experimental Arrangements

The transient response of the surge protective devices under study was investigated by using impulse current generators (Fig. 2a). For relatively low peak currents of 8/20 μs waveform (< 6 kA), a combination wave generator has been used (Hilo PG 12-804); an impulse current generator with interchangeable components has been employed for the generation of 10/350 μs, 1/130 μs and 8/20 μs (> 6 kA) waveforms, and the configuration and components are shown in Table II. Impulse currents were recorded using current transformers (Pearson 301X, Pearson 310), while the residual voltage of the SPD was monitored with the aid of a 400 MHz probe (LeCroy HVP 120) via twisted cables to minimize mutual inductance effects [28] (Fig. 2a).

The capacitive behavior of the SPDs was investigated by using a 4.8 kVA AC power supply (Agilent 6843A). The voltage at the SPDs terminals was recorded by a LeCroy PP008 500 MHz voltage probe, and the current was measured by employing high-power, low-inductance resistors, R_I, through a Tektronix P5205 A differential probe (50 MHz).

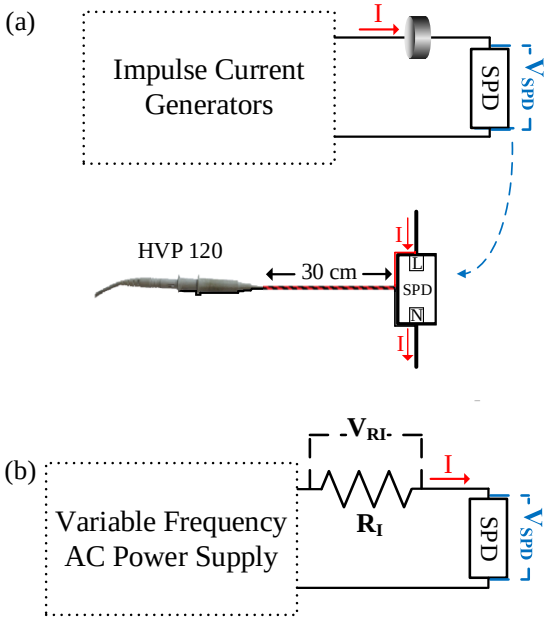

Fig. 2. Experimental arrangement: (a) Impulse currents, (b) Sinusoidal voltages.

TABLE II
IMPULSE CURRENT GENERATOR

Impulse Current	8/20 μs	10/350 μs	1/130 μs
C_{IC} (μF)	27	269	36
L_{IC} (μH)	2.7	11.5	2.5
R_{IC} (Ω)	0.36	1.9	5

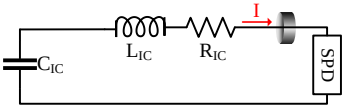

Current and voltage measurements were acquired in all cases by a 600 MHz digital oscilloscope (Tektronix TDS 3064B).

III. EXPERIMENTAL RESULTS AND ANALYSIS

Low-voltage surge protective devices exhibit a resistive, inductive, and capacitive transient behavior [20], [21]. This behavior is analyzed based on experimental results in what follows.

A. Resistive Behavior

Fig. 3 shows a typical residual voltage (L-N) of the single-pole SPD (Fig. 1) when conducting 10 kA, 8/20 μs impulse current. The voltage-current, *V-I*, characteristic of the SPD (L-N), can be obtained by using pairs of current, I_R, and residual voltage, V_R, at the time instant of $dI/dt = 0$ (peak of the surge current). Fig. 4 shows the *V-I* characteristic for a wide range of peak currents (30 A - 40 kA). The *V-I* characteristic of the SPD (L-N) is determined by the non-linear resistance of the SPD, *R(I)* that comprises (i) the non-linear resistance of the MOV [29] and (ii) the minor intrinsic resistance of the SPD conductive path. *V-I* is formulated as:

$$V(I) = a_5(Log(\mathrm{I}))^5 + a_4(Log(\mathrm{I}))^4 + a_3(Log(\mathrm{I}))^3 + a_2(Log(\mathrm{I}))^2 + a_1(Log(\mathrm{I}))^1 + a_0. \quad (1)$$

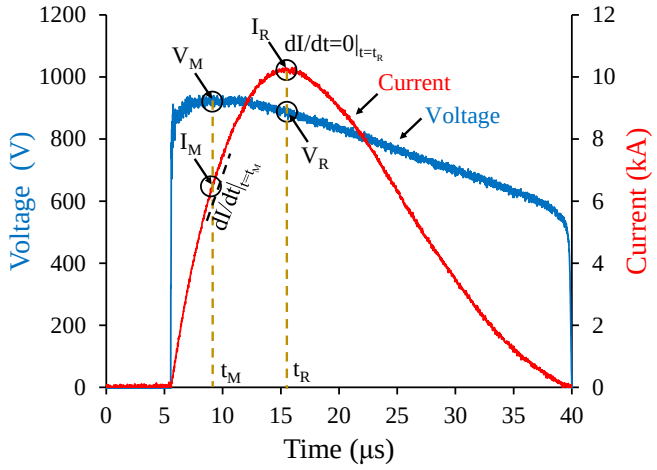

Fig. 3. Voltage at the single-pole SPD terminals (L-N); 10 kA, 8/20 μs.

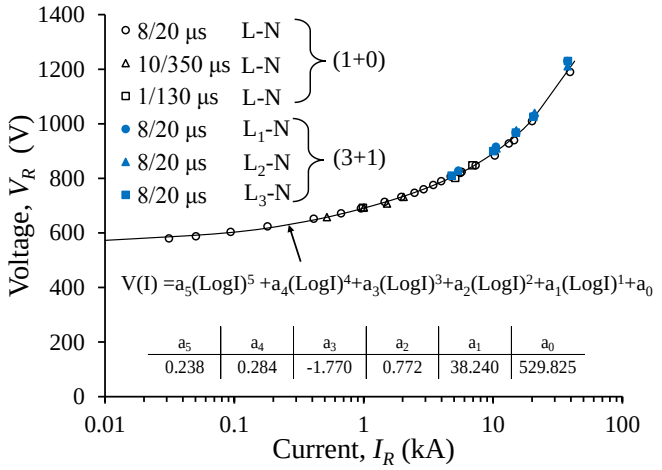

Fig. 4. Voltage-current (V_R, I_R) characteristic curve of the surge protective devices under study (1+0, 3+1).

It must be noted that the resistive behavior of the single-pole SPD (L-N) can be described by one voltage-current curve shown in Fig. 4, that is found to be practically independent of impulse current waveform (8/20 μs, 10/350 μs, 1/130 μs); a_0-a_5 factors in (1) were found from the best fitting curve of the experimental data (Fig. 4). This curve is also valid for the four-pole SPD since the effect of the intrinsic resistance of the conductive paths of the bases (1+0, 3+1) is minimal with respect to the non-linear resistance of the pluggable MOV-based modules. It is noteworthy that the pluggable modules were selected with the same $U_{1mA,}$ that is the DC voltage at which the module conducts 1 mA.

B. Inductive Behavior

Manufacturers commonly provide *V-I* characteristics of SPDs (L-N) based on maximum residual voltage, V_M, and peak current, I_R, that correspond to different time instants (t_M, t_R), as shown in Fig. 3. The fact that the residual voltage attains a maximum value at a current level, I_M, well before the peak of the current, I_R, signifies the inductive-like behavior of the SPD.

The maximum residual voltage can be formulated as:

$$V_M = \mathrm{R}(\mathrm{I_M})\,\mathrm{I_M} + \mathrm{L}\frac{dI}{dt}\Big|_{t=t_M} = \mathrm{R}(\mathrm{I_M})\,\mathrm{I_M} + (\mathrm{L}_{MOV} + \mathrm{L_{int}})\frac{dI}{dt}\Big|_{t=t_M}, \quad (2)$$

where I_M is the current at the time instant t_M, when the maximum residual voltage, V_M, occurs, $R(I_M)$ can be calculated based on (1), $dI/dt|_{t=t_M}$ is the current derivative at t_M, and L is the total SPD inductance along the surge current path. The latter consists of (i) L_{MOV}, that is the inductive-like behavior of the metal-oxide varistor, and (ii) L_{int}, that is the intrinsic inductance of the conductive paths between line and neutral. The varistor inductive-like behavior is associated with the dynamical response of the interfaces at the ZnO grain boundaries attributed in high fields mainly to the time needed for the holes to travel to the interfaces, where they reduce the negative charge and lower the potential barriers [12].

An experimental method for determining L_{int} is the replacement of the MOV modules of the SPD by aluminum/copper blocks according to [21] and measurement of the voltage at the terminals of the dummy SPD, V_D. Thus, L_{int} is given as:

$$L_{\mathrm{int}} = \left(V_D(\mathrm{t}) - \mathrm{R_D I(t)}\right) / \left(dI/dt\right), \quad (3)$$

where R_D is the intrinsic resistance of the dummy SPD. It is evident from Fig. 5 that the intrinsic inductance of the line to neutral path, L_{int}, of SPDs differs, and it can be deduced from (2) that this intrinsic inductance affects the maximum residual voltage, V_M, especially under high current derivative surge events. This is shown in Fig. 6, where for a given peak current, the maximum residual voltage occurs at L_1-N protection mode, which is associated with the longest surge path, thus also intrinsic inductance.

Fig. 7a shows the total inductance, L (L_{MOV}+L_{int}), of the

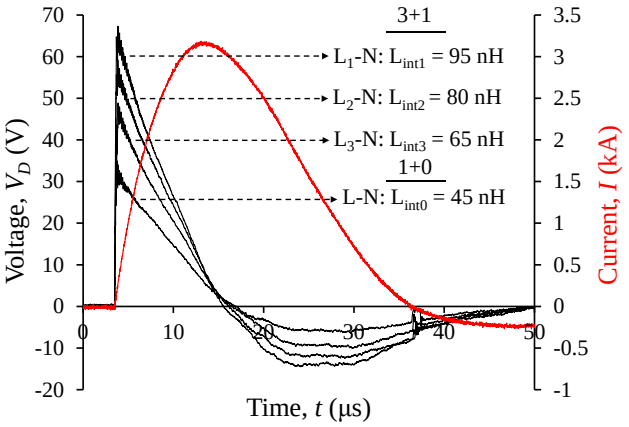

Fig. 5. Voltage at the dummy SPDs terminals (1+0, 3+1); 3 kA, 8/20 μs.

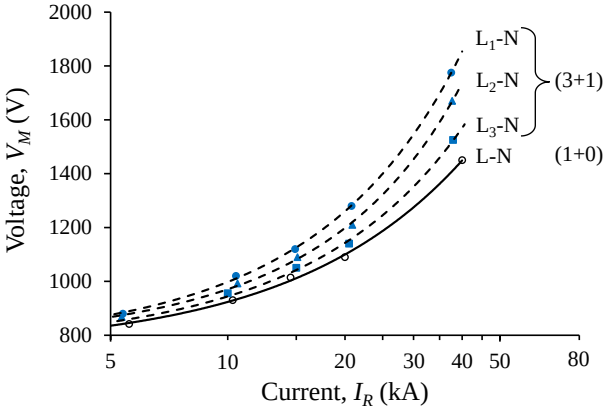

Fig. 6. Voltage-current (V_M, I_R) characteristic curve of the SPDs (1+0, 3+1).

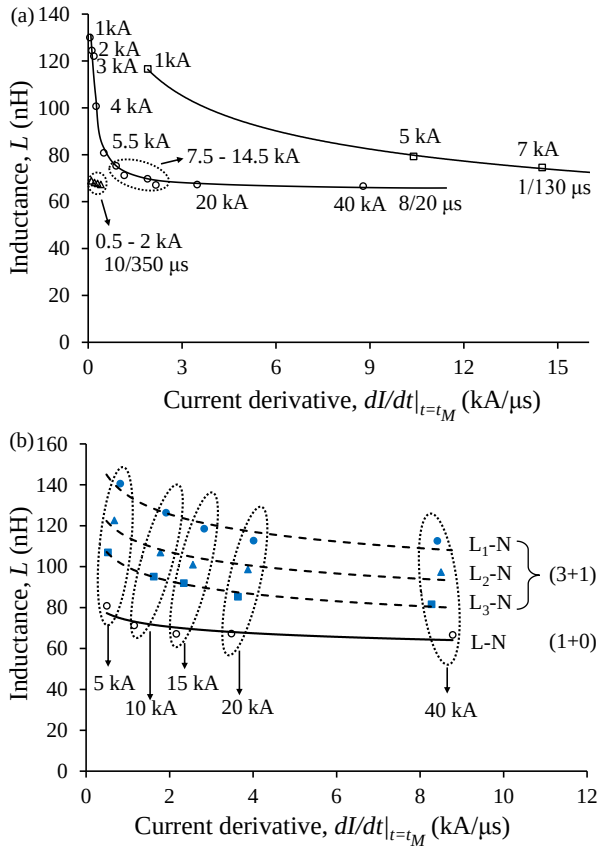

Fig. 7. Equivalent inductance of (a) the single-pole SPD (1+0) for different impulse current waveforms, (b) SPDs under study (1+0, 3+1) for 8/20 μs impulse current.

single-pole (1+0) SPD under study determined by (2) based on experimental records. It is evident that L depends on (i) impulse current waveform and (ii) current derivative; this supports the observations of variable inductive performance of MOVs, and MOV-based SPDs made by other researchers [12], [30], [31]. It must be noted that the different intrinsic inductances, L_{int0}-L_{int4}, shown in Fig. 5 are reflected in the equivalent inductances determined for the protection modes of single-pole (L-N) and four-pole SPD (L_1-N, L_2-N, L_3-N) under study (Fig. 7b).

C. Capacitive behavior

Sinusoidal voltages were applied between line and neutral terminals to determine the capacitive behavior of the SPDs. Current flow through the integrated MOV can be described as follows [32]:

$$I(t) = I_C(t) + I_R(t), \quad (4)$$

where $I_C(t)$ is the capacitive component and $I_R(t)$ is the resistive component of the current.

The MOV capacitance, $C_{L\text{-}N}$, can be estimated based on current and voltage derivative at the time instant of zero crossing of the voltage, t_0, as follows:

$$C_{L-N} = \frac{I_C(t_0)}{dV/dt|_{t=t_0}}, \quad (5)$$

where dV/dt and Ic are measured at t_0 when $I_R = 0$ in (5).

A variable $C_{L\text{-}N}$ value was found for a frequency range of 50 up to 1000 Hz, in line with previous measurements on varistors, [11], [32], [33] as shown in Fig. 8b. The effect of the SPD configuration was found negligible since the capacitive behavior of the SPD depends on the MOV-based pluggable module.

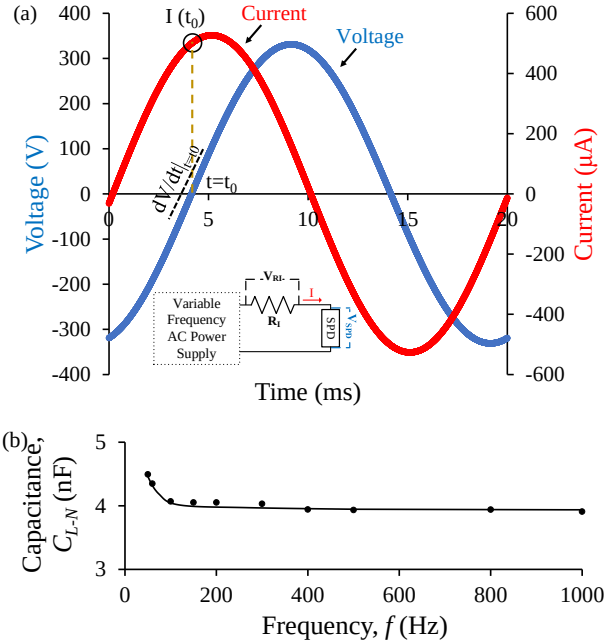

Fig. 8. Capacitive behavior of the SPDs under sinusoidal voltages (AC: 240V rms /50 Hz).

IV. Modeling Approach

A. ATP-EMTP Model

The line to neutral protection mode of surge protectives devices (SPDs) under study (Fig. 1) can be modeled by using the equivalent circuit shown in Fig. 9, that is integrated into the ATP-EMTP environment [34] by applying the parameters of Table III with time step, ΔT, of 1 ns. Although, this simplified lumped-circuit model considers a constant, rather than a dynamic inductance and capacitance, it satisfactorily describes the transient behavior of the SPDs on the frequency range and peak current amplitudes that were considered in this work. The determined inductance L at 20 kA, 8/20 μs (nominal discharge current, Fig. 7), the capacitance $C_{L\text{-}N}$ at 240 V/50 Hz (nominal system voltage, Fig. 8) and the non-linear resistance determined by impulse current experiments (equation 1, Fig. 4) have been adopted; the intrinsic inductance of the sections of line to neutral surge paths of SPDs (L_D, L_{N12}, L_{N23}, L_{N3N}) can be estimated based on surge tests to dummy SPDs (Fig. 5) by employing equations (a-d) shown in Fig. 9. It is noted that damping resistors R_p and R_s are used in parallel to inductances and in series to capacitances, respectively, to avoid numerical oscillation in ATP-EMTP (Fig. 9 and Table III), which employs the trapezoidal integration rule as a numerical solution method.

A validation of the proposed model is shown in what follows for surge events almost reaching the discharge current limit (40 kA, 8/20 μs) and maximum energy absorption capability (2 kA, 10/350 μs) that do not trip the internal thermal disconnector [35] (θ in Fig.1). Also, very fast-front (non-standard) impulse currents of 1/130 μs waveform were used for validation purposes, which are challenging in terms of the reproduction of SPD transient response in the sub-microsecond range.

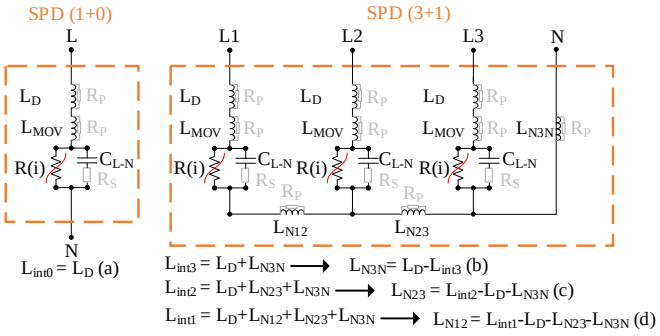

$R_p = K_p \cdot 2 \cdot L/\Delta T$, $R_s = K_s \cdot \Delta T/2 \cdot C$ [36]

Fig. 9. ATPDraw model of the surge protective devices under study.

TABLE III
ATP-EMTP MODELING OF THE SPDS

Element	Modeling Approach	Input			
R(i)	Branch nonlinear type 92 resistor	$R(I) = [a_5(LogI)^5 + a_4(LogI)^4 + a_3(LogI)^3 + a_2(LogI)^2 + a_1(LogI)^1 + a_0]/I$			
L (L_{MOV}+L_{int})	Branch linear inductor, damping factor K_p = 7.0	L-N	L_1-N	L_2-N	L_3-N
		70 nH	120 nH	105 nH	90 nH
C_{L-N}	Branch linear capacitor, damping factor K_s = 0.15	4.5 nF			

a_5	a_4	a_3	a_2	a_1	a_0
0.238	0.284	-1.770	0.772	38.240	529.825

L_{MOV}	L_D	L_{N12}	L_{N23}	L_{N3N}
25 nH	45 nH	15 nH	15 nH	20 nH

B. Validation and Discussion

The developed model (Fig. 9 and Table III) is implemented into the ATP-EMTP environment in order to validate its efficiency through comparison with experimental data. Fig. 10 shows the residual voltage records from impulse current tests together with simulation results. The computed residual voltage of the SPDs (V_M, V_R as defined in Fig. 3) is in satisfactory agreement with experimental records yielding errors less than 7% (Table IV) for impulse currents up to 40 kA, 8/20 μs, 2 kA, 10/350 μs (Fig. 10b) and 7 kA, 1/130 μs (Fig. 10c).

As it can be deduced from Fig. 10a and the inset graph of Fig. 10c, the measurement of the residual voltage at the wavefront of the impulse current (high *dI/dt*, *dV/dt*) can be challenging [37]; a satisfactory prediction of the residual voltage at such cases is feasible with the proposed time-domain modeling approach. Thus, the proposed model can be used for overcoming challenges mainly associated with the voltage measuring system and employed as an engineering tool for the prediction of (i) the residual voltage at the nominal discharge current (20 kA, 8/20 μs shown in Fig. 10a) determining the protection level, U_p, of SPD, and (ii) the highest crest value of the residual voltage, U_{max}, at the maximum discharge current (I_{max} = 40 kA, 8/20 μs) determining the required clearances per IEC 61643-11 [25].

It is noteworthy that the proposed model predicts the development of a maximum residual voltage (V_M ~ 1.6 kV) beyond the declared protection level ($U_p \leq$ 1.5 kV at 20 kA, 8/20 μs) of the SPD for 7 kA, 1/130 μs (inset graph Fig. 10c). This overshoot is important when considering the efficiency of SPDs in protecting sensitive electronic equipment (withstand voltage level of 1.5 kV) at very fast-front transients, such as subsequent lightning strokes [38] and nuclear electromagnetic pulses [39], [40]. To evaluate the effectiveness of the proposed model in reproducing the SPDs transient behavior, an additional comparison is made for the energy absorption, *E*, defined as:

$$E = \int V_{SPD}(t) I(t) dt, \quad (6)$$

where $V_{SPD}(t)$ is the voltage across the SPDs during surge current flow, $I(t)$. The proposed model results are in very good agreement with recorded energy absorption, that is one of the main parameters determining the SPD failure probability [11]; simulation errors on *E* are generally lower 7%. These results are

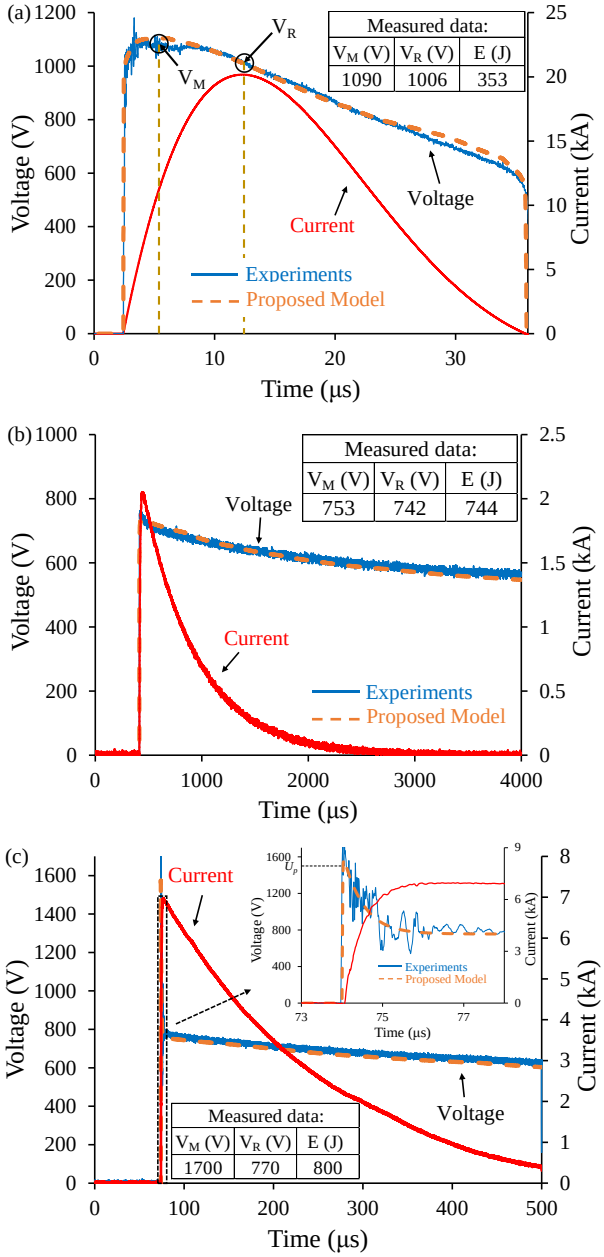

Fig. 10. Voltage and current at the single pole (1+0) SPD at L-N protection mode: (a) In: 20 kA, 8/20 μs, (b) 2 kA, 10/350 μs and (c) 7 kA, 1/130 μs.

TABLE IV
SIMULATION ERRORS IN RESIDUAL VOLTAGE AND ENERGY ABSORPTION OF THE SURGE PROTECTIVE DEVICES

Waveform	DIN rail SPD	Protection mode	Peak Current (kA)	Proposed model		
				Errors in		
				V_M[a] e_a(%)	V_R[b] e_b(%)	E[c] e_c(%
8/20 µs	(1+0)	L-N	1.0	0.77	-0.21	-0.08
	(1+0)	L-N	2.0	0.60	0.67	-2.33
	(1+0)	L-N	3.0	0.88	0.24	-0.63
	(1+0)	L-N	4.0	0.68	0.21	-1.28
	(1+0)	L-N	5.5	0.14	0.34	-2.76
	(3+1)	L_1-N	5.0	1.93	1.09	1.20
	(3+1)	L_2-N	5.0	0.92	0.73	1.45
	(3+1)	L_3-N	5.0	0.83	0.25	0.26
	(1+0)	L-N	7.5	0.27	0.88	-1.36
	(1+0)	L-N	10	-0.12	-0.05	-0.82
	(3+1)	L_1-N	10	0.69	2.30	1.17
	(3+1)	L_2-N	10	-0.71	2.52	0.18
	(3+1)	L_3-N	10	0.62	1.88	0.29
	(1+0)	L-N	13	-0.39	0.55	-0.18
	(1+0)	L-N	15	-0.77	0.46	-1.56
	(3+1)	L_1-N	15	-0.89	2.37	1.56
	(3+1)	L_2-N	15	-2.20	1.77	1.17
	(3+1)	L_3-N	15	-0.57	1.04	0.03
	(1+0)	L-N	20	-1.32	-0.28	-0.81
	(3+1)	L_1-N	20	-2.76	0.97	0.80
	(3+1)	L_2-N	20	-3.88	1.17	1.08
	(3+1)	L_3-N	20	-1.91	1.17	0.32
	(1+0)	L-N	40	-1.97	1.66	-0.41
	(3+1)	L_1-N	40	-3.83	1.92	0.85
	(3+1)	L_2-N	40	-4.82	-0.08	-1.49
	(3+1)	L_3-N	40	-4.79	-0.02	-0.99
	Max/Min Error (%):			**-4.82**	**2.52**	**-2.76**
	Average of Absolute Error[d], e_d (%):			**1.51**	**0.96**	**0.96**
10/350 µs	(1+0)	L-N	0.50	1.55	1.02	-4.76
	(1+0)	L-N	1.00	1.09	1.10	-4.34
	(1+0)	L-N	1.50	1.27	-0.38	-3.01
	(1+0)	L-N	2.00	2.47	1.07	-2.07
	Max/Min Error (%):			**2.47**	**1.10**	**-4.76**
	Average of Absolute Error[d], e_d (%):			**1.60**	**0.89**	**3.54**
1/130 µs	(1+0)	L-N	1.00	7.05	0.90	-6.51
	(1+0)	L-N	5.00	6.82	-0.55	-6.10
	(1+0)	L-N	7.00	6.44	1.52	-0.59
	Max/Min Error (%):			**7.05**	**1.52**	**-6.51**
	Average of Absolute Error[d], e_d (%):			**6.77**	**0.99**	**4.40**

$$e_a = \frac{V_M(\text{Measured}) - V_M(\text{Simulated})}{V_M(\text{Measured})} \cdot 100\% \qquad e_b = \frac{V_R(\text{Measured}) - V_R(\text{Simulated})}{V_R(\text{Measured})} \cdot 100\%$$

$$e_c = \frac{E(\text{Measured}) - E(\text{Simulated})}{E(\text{Measured})} \cdot 100\% \qquad e_d = \sum_{n=1}^{N} |\text{error}| \Big/ N$$

very encouraging, when considering that the measurement error of voltage and current records is within 3% and that voltage-current characteristics of metal-oxide varistors (MOVs) of the same type may vary up to 10% [41].

The proposed model, validated against a wide range of impulse currents, can be used for (i) insulation coordination studies and (ii) dimensioning of SPDs against lightning-related overvoltages; these are hot topics in recent research work on surge protection [42]-[44].

V. CONCLUSIONS

A simplified electromagnetic transient model has been developed for DIN rail surge protective devices (SPDs) employing metal-oxide varistors (MOVs) based on impulse current experiments. A comparison of the simulation results derived from the developed ATP-EMTP model with experimental data has shown that:

- The resistive behavior of the SPD can be modeled by a non-linear resistance derived from the voltage-current curve drawn from voltage/current records acquired at the time instant of the surge current peak. This non-linear resistance was found practically independent of SPD configurations (1+0, 3+1) and impulse current waveforms (8/20 µs, 10/350 µs, 1/130 µs).
- The adoption of a constant capacitance and inductance for representing the dynamic capacitive and inductive behavior of the SPD, although it is a simplified approach, it provides satisfactory results in terms of the surge response of the SPDs. In case of surge currents (> 0.5 kA), the inductive behavior dominates and masks the capacitive behavior of the SPD; the use of a constant inductance obtained from the nominal discharge current, and a capacitance value derived from the nominal system voltage and power frequency proved satisfactory.
- The maximum residual voltage of SPD, which affects the efficiency of surge protection offered to the equipment, depends significantly on the SPD configuration (1+0 base or L_1-N, L_2-N, L_3-N in 3+1 base). This is because the intrinsic inductance of each surge current path is different and decisive on the residual voltage overshoot in case of high current derivative surge events such as 40 kA, 8/20 µs and 7 kA, 1/130 µs. For low current derivative impulse currents, the effect of the SPD configuration is minimal and masked by the inductive-like performance of the MOVs. Thus, the use of different inductances per protection mode (L-N, L_1-N, L_2-N, L_3-N) is suggested for an accurate representation of the inductive behavior of SPDs; the intrinsic inductance of the line to neutral surge current path can be determined based on surge tests of dummy SPDs with nonlinear elements replaced by aluminum blocks.
- The proposed model yields satisfactory results for a wide range of standard (1 - 40 kA, 8/20 µs & 0.5 - 2 kA, 10/350 µs) and non-standard (very fast-front) impulse currents (1 - 7 kA, 1/130 µs) with simulation errors generally less than 7% in the SPDs maximum residual voltage and the associated energy absorption.

The proposed model, validated against a wide range of impulse currents, can be used for insulation coordination studies and dimensioning of SPDs against lightning-related overvoltages.

VI. Acknowledgment

Prof. Thomas Tsovilis would like to thank Mr. Andrej Pirih and Mrs. Mirjam Cergolj for their insightful discussions on the transient response of SPDs employing varistors and Mr. Thomas Kohushölter, Head of VDE Testing and Certification Institute in Berlin, for their conversations on the determination of voltage protection level of SPDs, U_p, and the maximum voltage, U_{max}, for clearance determination per IEC 61643.

VII. References

[1] Y. Baba and V. A. Rakov, *Lightning-induced effects in electrical and telecommunications systems*, 1st ed., London, United Kingdom: IET Energ. Eng. Ser. 114, 2020.

[2] A. Borghetti and C. A. Nucci, "Integration of distributed energy resources in distribution power systems," in *Integration of Distributed Energy Resources in Power Systems*, 1st ed., T. Funabashi, Ed. Academic Press, 2016, pp. 16-50.

[3] German Insurance Association, Blitzbilanz 2021: Anzahl und Höhe der Schäden steigen, Link, Accessed Mar. 2023.

[4] B. M. Buchholz and Z. A. Styczynski, *Smart Grids: Fundamentals and Technologies in Electric Power Systems of the Future*, 2nd ed., Springer-Verlag Berlin Heidelberg, 2020.

[5] A. Borghetti, W. A. Chisholm, F. Napolitano, C. A. Nucci, F. Rachidi, and F. Tossani, "Software tools for the lightning performance assessment," in *Lightning Interaction with Power Systems - Volume 2: Applications*, 1st ed., A. Piantini, Ed. London, United Kingdom: IET Energ. Eng. Ser. 172, 2020, pp 425-452.

[6] H. Tang, V. Scuka, M. Cergolj, and M. Trontelj, "Transient control characteristics of low voltage varistors,"in *Proc. 1995 Int. Conf. Contr. Autom. Elect. Pow. Syst.: VAES-95*, Ljubljana, Slovenia, 1995, pp. 1-10.

[7] Z. Topcagic, M. Mlakar and T. E. Tsovilis, "Electrothermal and overload performance of metal-oxide varistors," *IEEE Trans. Power Del.*, vol. 35, no. 3, pp. 1180-1188, June 2020.

[8] Q. Zhou, H. Yang, X. Huang, M. Wang, and X. Ren, "Numerical modelling of MOV with Voronoi network and finite element method," *IET Hig. Volt.*, pp. 1–8, 2021.

[9] T. Noda, "XTAP," in *Numerical Analysis of Power System Transient and Dynamics*, 1st ed. A. Ametani, Ed. London, United Kingdom: IET Energ. Eng. Ser. 78, 2015, pp. 169-211.

[10] R. Araneo, *Advanced Time Domain Modelling for Electrical Engineering*, 1st ed., London, United Kingdom: Institute of Engineering and Technology, 2022.

[11] J. He, *Metal Oxide Varistors: From Microstructure to Macro-Characteristics*, 1st ed., Wiley-VCH Verlag GmbH and Co. KGaA, 2019.

[12] F. Greuter, "ZnO Varistors: From grain boundaries to power applications," in *Oxide Electronics*, 1st ed., A. Ray, Ed. London, United Kingdom: JohnWil. and Sons Ltd, 2021, pp. 157-234.

[13] P. N. Mikropoulos, T. E. Tsovilis, Z. Politis and A. G. Kagiannas, "Evaluation of fast-front overvoltages arising at a 20/0.4 kV distribution transformer, " in *Proc. 2010 7th Med. Conf. Exh. Pow. Gen., Trans., Dist. and Energ. Conv.*, Agia Napa, Cyprus, 2010, pp 1-6.

[14] Z. He and Y. Du, "SPD protection distances to household appliances connected in parallel, " *IEEE Trans. Electromagn. Compat.*, vol. 56, no. 6, pp. 1377-1385, Dec. 2014.

[15] P. Pinceti and M. Giannettoni, "A simplified model for zinc oxide surge arresters," *IEEE Trans. Power Del.*, vol. 14, no. 2, pp. 393–398, Apr. 1999.

[16] F. Fernandez and R Diaz, "Metal- oxide surge arrester model for fast transient simulations, " in *Proc. 2001 Int. Conf. Pow. Syst. Trans.*, Rio De Janeiro, Brazil, 2001, pp. 20–24.

[17] V. S. Brito, G. R. S. Lira, E. G. Costa, and M. J. A. Maia, "A wide-range model for metal-oxide surge arrester*," IEEE Trans. Dielectr. Electr. Insul.*, vol. 33, no. 1, pp. 102–109, Feb. 2018.

[18] A. Pirih and A. Pregelj, "Contribution to mathematical modelling of metal oxide surge arresters based on exact analysis of parasitic inductive influences," *in Proc. 40th Int. Conf. Microelectr., Dev. Mat.*, Maribor, Slovenia, 2004, pp. 225–230.

[19] R. Montaño, M. Edirisinghe, V. Cooray, and F. Roman, "Behavior of low-voltage surge protective devices under high-current derivative impulses," *IEEE Trans. Power Del.*, vol. 22, no. 4, pp. 2185–2190, Oct. 2007.

[20] T. E. Tsovilis, A. Y. Hadjicostas, E. T. Staikos, and G. D. Peppas "Modeling the transient behavior of surge protective devices connected to the DC side of electric vehicle charging stations," *in Proc. IEEE IAS Annu. Meet.*, Detroit, MI, USA, Oct. 2022.

[21] T. E. Tsovilis, "Critical insight into performance requirements and test methods for surge protective devices connected to low-voltage power systems," *IEEE Trans. Power Del.*, vol. 36, no. 5, pp. 3055-3064, 2021.

[22] Y. Men, X. Lu, Z. Zhang and R. Thiagarajan, "Metal oxide varistor (MOV) lifetime estimation with impulse-based testing in PV inverter systems," in *Proc. 2022 IEEE 13th Int. Symp. Pow. Elect. Dist. Gen. Syst.*, Kiel, Germany, 2022, pp. 1-4.

[23] Y. Méndez Hernández et al., "A simulation approach on rotor blade electrostatic charging and its effect on the lightning overvoltages in wind parks, " *Elec. Power Sys. Res.*, vol. 139, pp. 22-31, Oct. 2016.

[24] Q. Sun, et. al., "A comprehensive lightning surge analysis in offshore wind farm," *Elec. Power Sys. Res.*, vol. 211, pp. 1-17, Oct. 2022.

[25] IEC 61643-11, *Low-voltage surge protective devices - Part 11: Surge protective devices connected to low-voltage power systems - Requirements and test methods*, Ed. 1, 2011.

[26] IEC 61643-12, *Low-voltage surge protective devices - Part 12: Surge protective devices connected to low-voltage power systems - Selection and application principles*, Ed. 3, 2020.

[27] IEC 60364-5-53, *Low-voltage electrical installations - Part 5-53: Selection and erection of electrical equipment - Devices for protection for safety, isolation, switching, control and monitoring*, Ed. 4, 2019.

[28] OSM/IN 288 for EN 61643 series + EN 50539 series "General instruction for residual voltage measurements," Decided 2018 (meeting 28).

[29] E. T. Staikos, G. D. Peppas and T. E. Tsovilis, "Wide frequency response of varistors and coordination with transient voltage suppression diodes, " *IEEE Trans. Power Del*., 2022, Early access.

[30] I. Kim, T. Funabashi, H. Sasaki, T. Hagiwara, and M. Kobayashi, "Study of ZnO arrester model for steep front wave," *IEEE Trans. Power Del.*, vol. 11, no. 2, pp. 834–841, Apr. 1996.

[31] H. Chen and Y. Du, "A comprehensive study on the nonlinear behavior of metal oxide varistors," in *Proc. 2016 33rd Int. Conf. Lightn. Protect.*, Estoril, Portugal, 2016, pp. 1-5.

[32] E. T. Staikos and T. E. Tsovilis, "Low-frequency response of low-voltage metal-oxide varistors used for telecommunication systems protection," in *Proc. 2020 21st Int. Conf. Hi. Volt. Eng. Appl*., pp. 1-4.

[33] Y. T. Katharina, " Electrothermal Modeling, Simulation and Optimization of Surge Arresters," Ph.D. dissertation, Dept. Electr. Eng. Inform. Techn., Univ. Darmstad, 2020.

[34] H. K. Høidalen, L. Prikler, and F. Penaloza, *ATPDraw version 7.3 for Windows Users' Manual*, NTNU Norway, 2021.

[35] Q. Zhou, T. Cao, Y. Liu, X. Huang, and X. Bian, "Microstructure Observation, Accumulated Equivalent Stress and Creep Strain Simulation of SPD Disconnector Solder Joint Based on Isothermal Aging," *IEEE Trans. Comp., Pac. Man. Tech.*, vol. 12, no. 11, pp. 1771-1780, Nov. 2022.

[36] H. W. Dommel, Electro-Magnetic Transients Program (EMTP) Theory Book, Portland, OR: Bonneville Power Administration, 1986.

[37] K. Schon, *High voltage measurement techniques: Fundamentals, measuring instruments, and measuring methods*, 1st ed., Switzerland, Springer, 2019.

[38] CIGRE Working Group C4.408, *Lightning protection of low-voltage networks*, Technical Brochure 550, Aug. 2013.

[39] MIL-STD-188-125-1, *High-altitude electromagnetic pulse (hemp) protection for ground-based c4i facilities performing critical, time-urgent missions part 1, fixed facilites*, US Department of Defence,1999.

[40] Electromagnetic Pulse (EMP) Protection and Resilience Guidelines for Critical Infrastructure and Equipment, National Coordinating Center for Communications (NCC), National Cybersecurity and Communications Integration Center Arlington, Virginia, Feb. 2019, Unclassified.

[41] EPCOS Databook 2018, Link, accessed Mar. 2023.

[42] T. Bowman, M. Halligan, and R. LIannes, "High-Frequency Metal-Oxide Varistor Modeling Response to Early-time Electromagnetic Pulses," in *Proc. Int. Symp. Electr. Comp. & Sig./Pow. Int. (EMCSI)*, Reno, NV, USA, 2020.

[43] S. Chen et al., "Surge protective device failure caused by triggered lightning continuing current and M component*," Elec. Pow. Sys. Res. Vol.*, vol. 218, May 2023.

[44] N. Dong et al., "An Equation-based Dynamic Nonlinear Model of Metal-Oxide Arrester and its Spice Implementation," *IEEE Trans. Cir. Sys. II: Exp. Br.*, Early Access, 2023. DOI: 10.1109/TCSII.2023.3245300